membranes

MDPI

Article

Hydrogen (H_2)/Toluene (TOL) Separation via One and Two Stages of the Bis(triethoxysilyl)ethane (BTESE) Membranes

Suhaina Mohd Ibrahim [1,*], Xin Yu [1], Shigeru Miyata [1], Kengo Mishina [1], Feridoun Salak [1], Sulaiman Oladipo Lawal [1], Toshinori Tsuru [1,2,*] and Ken-ichi Sawamura [1,*]

[1] eSep Inc., Keihanna Open Innovation Center@Kyoto (KICK), Annex 320, 7-5-1, Seikadai, Seika-cho, Soraku-gun, Kyoto 619-0238, Japan; sulaiman@esep.co.jp (S.O.L.)
[2] Department of Chemical Engineering, Hiroshima University, 1-4-1 Kagamiyama, Higashihiroshima 739-8527, Japan
* Correspondence: suhaina@esep.co.jp (S.M.I.); tsuru@esep.co.jp (T.T.); sawamura@esep.co.jp (K.-i.S.)

Abstract: The separation ability of bis(triethoxysilyl)ethane (BTESE) membranes for hydrogen (H_2) purification from hydrogen (H_2)/toluene (TOL) gas mixtures after a methylcyclohexane (MCH) dehydrogenation process was investigated via one-stage and two-stage membrane processes. This study revealed that BTESE membranes of varied pore sizes (0.4, 0.5, and 0.7 nm) in a one-stage configuration can manage to achieve a H_2 purity ~99.9%. However, the TOL concentrations fell within a wide range, ranging from 280 to 5441 ppm. A primary goal of this research was to lower the TOL concentration in the permeate stream below 200 ppm. Hence, by applying the two-stage membrane, it was demonstrated that the TOL concentration in the permeate stream could be lowered below 200 ppm.

Keywords: hydrogen purification; hydrogen (H_2)/toluene (TOL) gas mixtures; bis(triethoxysilyl)ethane (BTESE) membranes

check for updates

Citation: Ibrahim, S.M.; Yu, X.; Miyata, S.; Mishina, K.; Salak, F.; Lawal, S.O.; Tsuru, T.; Sawamura, K.-i. Hydrogen (H_2)/Toluene (TOL) Separation via One and Two Stages of the Bis(triethoxysilyl)ethane (BTESE) Membranes. *Membranes* **2024**, *14*, 165. https://doi.org/10.3390/membranes14080165

Academic Editor: Kew-Ho Lee

Received: 7 May 2024
Revised: 12 July 2024
Accepted: 23 July 2024
Published: 25 July 2024

Copyright: © 2024 by the authors. Licensee MDPI, Basel, Switzerland. This article is an open access article distributed under the terms and conditions of the Creative Commons Attribution (CC BY) license (https://creativecommons.org/licenses/by/4.0/).

1. Introduction

Hydrogen (H_2) is one of the potential renewable energy sources of the future [1–5]. The International Energy Agency (IEA) predicts that the world's need for H_2 will increase seven-fold to 520 Mt by 2070 [6]. Various types of inorganic membranes, such as metal, molecular sieving carbon, zeolites, and ceramic membranes [7–9], have been considered for H_2 separation. As one of the new classes of membranes, organosilica membranes, especially BTESE-derived membranes, have been extensively investigated for the last decade since they show excellent H_2 permeance (H_2 permeance > 10^{-6} mol m^{-2} s^{-1} Pa^{-1} and H_2/TOL > 1000) [10,11]. In the present study, the pore size distribution of our BTESE membranes was controlled by altering the number of coating layers of the BTESE solution [12,13] instead of focusing on different water ratios [14–16], firing temperature [17,18], doping with ZIF-7 [19], and copolymerization [20]. Previously, our membrane was successfully used in the separation of DMF and H_2O [13]. Hence, we believe our in-house membranes are capable of H_2/TOL separation as well.

Since H_2 cannot be obtained directly from nature, it is a secondary energy source. Green H_2 is produced by water electrolysis using electricity generated from solar or wind energy, whereas blue hydrogen is extracted alongside the CO_2 emitted from the hydrocarbons in fossil fuels [21–23]. For both types of H_2, the greatest difficulties in expanding the use of H_2 energy are safe storage and transportation. To overcome this barrier, organic chemical hydrides such as methylcyclohexane (MCH) are proposed as hydrogen carriers because of their ease of handling.

It is well known that MCH, which catalytically decomposes to H_2 and TOL, liquefies at room temperature and has a volume equivalent to several hundred thousandths of H_2. Since MCH is stable at normal temperatures, it can be utilized in the existing fuel supply

chain, including gas stations. Hence, H_2 and TOL need to be separated at the use site. This is achieved by vaporizing the MCH and catalytic decomposition at 250–300 °C, followed by purification or separation of H_2 and TOL using a ceramic membrane [14,24–30]. To achieve a high purity of H_2, a typical process includes the condensation of decomposed MCH to separate gas (H_2) and liquid product (TOL) from the MCH dehydrogenation reaction, followed by the purification of H_2 gas from that containing saturated TOL vapor.

However, most of the researchers are focusing on the BTESE and silica membrane reactors coupled with catalysts [14,25–28] for the dehydrogenation of methylcyclohexane (MCH) to toluene (TOL). Only limited studies have been reported focusing on the production of high-purity H_2 from the H_2/TOL mixture. In the present study, we used H_2 and TOL as our feed components instead of MCH. It is well known that H_2 separation membranes can be used in two ways. The first approach involves a membrane for a one-stage purification process after the MCH dehydrogenation reaction. However, a one-stage membrane of extremely high selectivity is required to achieve the minimal specification of fuel cell application. So as another approach, a two-stage membrane is proposed for further purification. As the main goal of this study is to achieve H_2 purity > 99.9% and a TOL concentration in the permeate stream below 200 ppm, the present study will only focus on the one-stage and two-stage BTESE membrane systems by using our own in-house-produced BTESE membrane.

2. Materials and Methods

2.1. Preparation of BTESE-Derived Sols and Membranes

The organosilica precursor BTESE was dissolved in an ethanol (EtOH) solution. After that, under vigorous agitation, dropwise additions of nitric acid (HNO_3) and H_2O were made with the final molar ratios of BTESE/H_2O/HNO_3 = 1/240/0.2. The concentration of BTESE was maintained at 5 weight percent (wt.%) by adjusting the amount of EtOH added to the solutions. After 6 h of continuous stirring at 25 °C, the solution was stored in a closed system to allow BTESE-derived organosilica sols to develop. It was then aged for 8 days at 50 °C before being used as a top layer.

Porous α-alumina tubes with an outer diameter of 12 mm and 400 mm in length, 50% porosity, and an average pore size of 3 μm were used as a support. The porous support was supplied by IWAO JIKI KYOGYO Co., Ltd., Saga Prefecture, Japan [12]. The exterior of the porous support was first covered with α-alumina particles, which had an average diameter of 0.2 μm. After that, the surface was fired for ten minutes at 550 °C to produce an α-alumina particle layer. Ultimately, the BTESE solution was coated, dried, and fired for 30 min at 300 °C under air to form the BTESE-derived organosilica top layer. Our previous manuscripts [12,13] provide a comprehensive overview of the membrane fabrication procedure.

In the present study, BTESE membranes are referred to as BTESE-x-y. The x and y letters indicate the membrane pore size and the membrane serial number, respectively, as shown in Figure 1. In the present study, there is 1 membrane with a pore size around 0.7 nm and another with a pore size around 0.5 nm and 4 membranes with a pore size around 0.4 nm, and Table 1 lists all the membranes that were used in this study. The morphologies of the BTESE membranes were examined using a Hitachi S-48000 field emission scanning electron microscope (FESEM)Hitachi High-Tech, Tokyo, Japan. Figure 2 shows a SEM image of a cross-section of an in-house-prepared BTESE membrane. This clearly shows that a crack-free continuous separation layer thickness below 3 μm was formed on the top of the intermediate and alumina layers after the calcination process at 300 °C. Other characterizations can be found elsewhere [11,14,16].

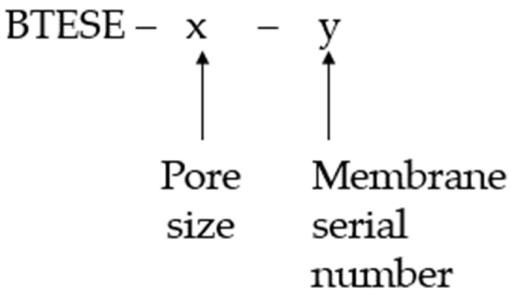


Figure 1. BTESE sample coding.

Table 1. List of membrane samples.

Membrane Lists	Coating Times of Top Layers	BTESE Sols for Top Layers
BTESE-0.7-1	4	1 wt.% BTESE sol after aging for 8 days at 50 °C
BTESE-0.5-1	5	
BTESE-0.4-1 BTESE-0.4-2 BTESE-0.4-3 BTESE-0.4-4	6	

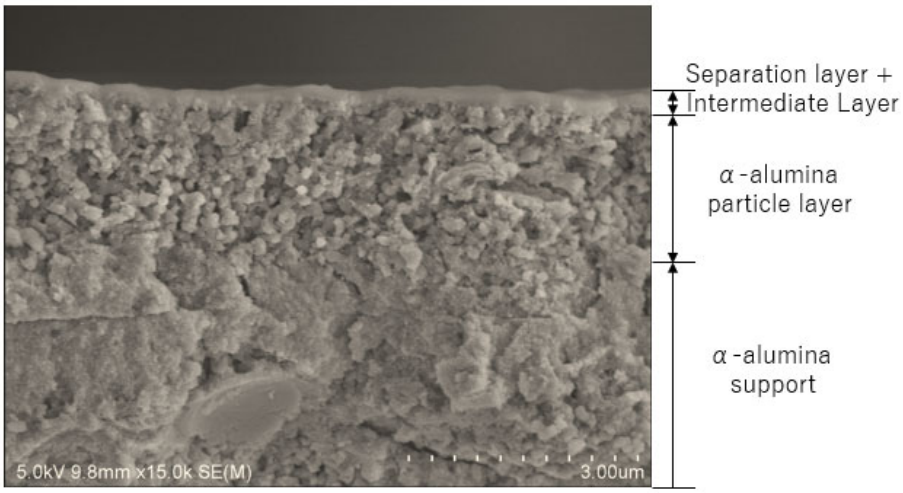


Figure 2. SEM image of a cross-section of a BTESE membrane.

2.2. Single-Gas Permeation (SGP)

The SGP measurement was carried out at 200 °C using single components of He, H_2, N_2, CH_4, CF_4, and SF_6. The permeate stream was kept at atmospheric pressure while the membrane module experienced a transmembrane pressure of 0.04–0.1 MPa. The gas permeance, P (mol m^{-2} s^{-1} Pa^{-1}), is obtained from Equation (1). The gas flowrates of the permeate streams were monitored using a mass flow meter (Kofloc EX-700R model, Kyoto, Japan) with flow rates up to 100 mL/min and 5 L/min, while the pressure of the retentate stream was measured by a digital pressure manometer (DMS-7A, 200 kPa, Hitachi High-Tech, Tokyo, Japan).

$$P = n/S\Delta p \quad (1)$$

Equation (1) uses n, or the permeate flow rate (mol s^{-1}), as its unit. S represents the membrane surface area (m^2) and Δp stands for the transmembrane pressure differential

(Pa). The ratio of gas permeance for A and B is defined as $\alpha_{A/B}$ (-) in Equation (2), which represents the optimal selectivity for A over B.

$$\alpha_{A/B} = P_A / P_B \quad (2)$$

2.3. H_2/TOL Separation Test

Figure 3a displays a schematic diagram of the one-stage gas separation device. The pressure of the feed (F1) stream was set at 200 kPaA and controlled using a needle valve. The pressure of the feed (F1) and retentate (R1) streams were measured by a digital pressure manometer (DMS-7A, 200 kPa, Hitachi High-Tech, Tokyo, Japan). The permeate (P1) stream was kept at atmospheric pressure. H_2 was supplied directly from a gas cylinder at a flowrate of 4.94 L/min, while TOL was fed using a pump (LC-10 AD VP Shimadzu, Liquid Chromatography, Tokyo, Japan) at a flowrate of 1.2 mL/min to control the feed concentration at 30,000 ppm. The H_2/TOL binary mixture was fed on the shell side of the membrane module, whose temperature was maintained at 200 °C. The gas flow rates of the feed (F1), retentate (R1), and permeate (P1) streams were monitored using a mass flow meter (Horiba, STEC, Z500 model). The Agilent 990 micro gas chromatography (Channel 1 Molsieve 5A (H_2 measurement) and Channel 3 CP-SIL 5CB (TOL measurement) were used to measure the gas compositions of the permeate (P1) stream. The gas compositions in the retentate (R1) were calculated from the material balance.

Figure 3b depicts the apparatus diagram for the two-stage gas separation equipment. Here, the pressure of the feed (F1) stream was set at 300 kPaA and controlled using the needle valve. H_2 and TOL were supplied similarly to the one-stage process (Figure 3a). The permeate (P1) stream from the first stage becomes the feed of the second stage, with a pressure between 111 kPaA and 133 kPaA. The pressure of the feed (F1), permeate (P1), retentate (R1), and permeate (P2) from second-stage streams were measured by a digital pressure manometer (DMS-7A, 200 kPa, Hitachi High-Tech, Tokyo, Japan). The feed H_2/TOL binary mixture flowed in the direction of the shell side of the membrane module, where the temperature was set at 200 °C. A mass flow meter (Horiba, STEC, Z500 model, Kyoto, Japan) was used to monitor the gas flow rates of the feed (F1), retentate (R1), and permeate (P2) streams. The gas compositions of the permeate (P2) and retentate (R2) streams were determined using Agilent 990 micro gas chromatography, Santa Clara, CA United States. The gas compositions in both permeate (P1) and retentate (R1) were calculated from the material balance.

Partial pressure distributions (concentration distributions) in mixed-gas permeation (one- and two-stage gas separation studies) are produced by selective permeation in the flow direction. Therefore, the driving force for permeation was determined using the logarithmic mean pressure difference for the component of i ($\Delta p_{i,lm}$):

$$\Delta p_{i,lm} = \frac{\Delta p_{i,\,in} - \Delta p_{i,out}}{ln\left(\frac{\Delta p_{i,in}}{\Delta p_{i,out}}\right)} \quad (3)$$

where $\Delta p_{i,\,in}$ and $\Delta p_{i,out}$ are the partial pressure difference of the *i*-component between the feed and the permeate stream at the inlet and at the outlet, respectively.

The H_2 purity in the permeate or retentate streams is defined as the ratio of the H_2 flowrate over total flowrate as follows.

$$H_2\ purity\ in\ permeate\ stream = \left(\frac{Q_{p,\ H_2}}{Q_{t,p}}\right).(100\%) \quad (4)$$

$$H_2\ purity\ in\ retentate\ stream = \left(\frac{Q_{r,\ H_2}}{Q_{t,r}}\right).(100\%) \quad (5)$$

where Q_{p,H_2}, $Q_{t,p}$, Q_{r,H_2}, $Q_{t,r}$ are expressed in mol/s, respectively.

The H_2 recovery in the permeate stream is defined as the amount of H_2 recovered as the product in the permeate stream, while TOL recovery is defined as the amount of the product recovered in the retentate stream.

$$H_2 \text{ recovery in permeate stream} = \left(\frac{(x_{p,\ H_2})(Q_{t,p})}{\left(x_{f,\ H_2}\right)\left(Q_{t,f}\right)} \right) \quad (6)$$

$$TOL \text{ recovery in retentate stream} = \left(\frac{(x_{r,\ TOL})(Q_{t,r})}{\left(x_{f,\ TOL}\right)\left(Q_{t,f}\right)} \right) \quad (7)$$

where the $x_{p,\ H_2}$, $x_{r,\ TOL}$, $x_{f,\ H_2}$ and $x_{f,\ TOL}$ are expressed in mol fraction while $Q_{t,p}$, $Q_{t,r}$ and $Q_{t,f}$ are the flowrates in permeate, retentate, and feed streams, respectively, in L/min unit.

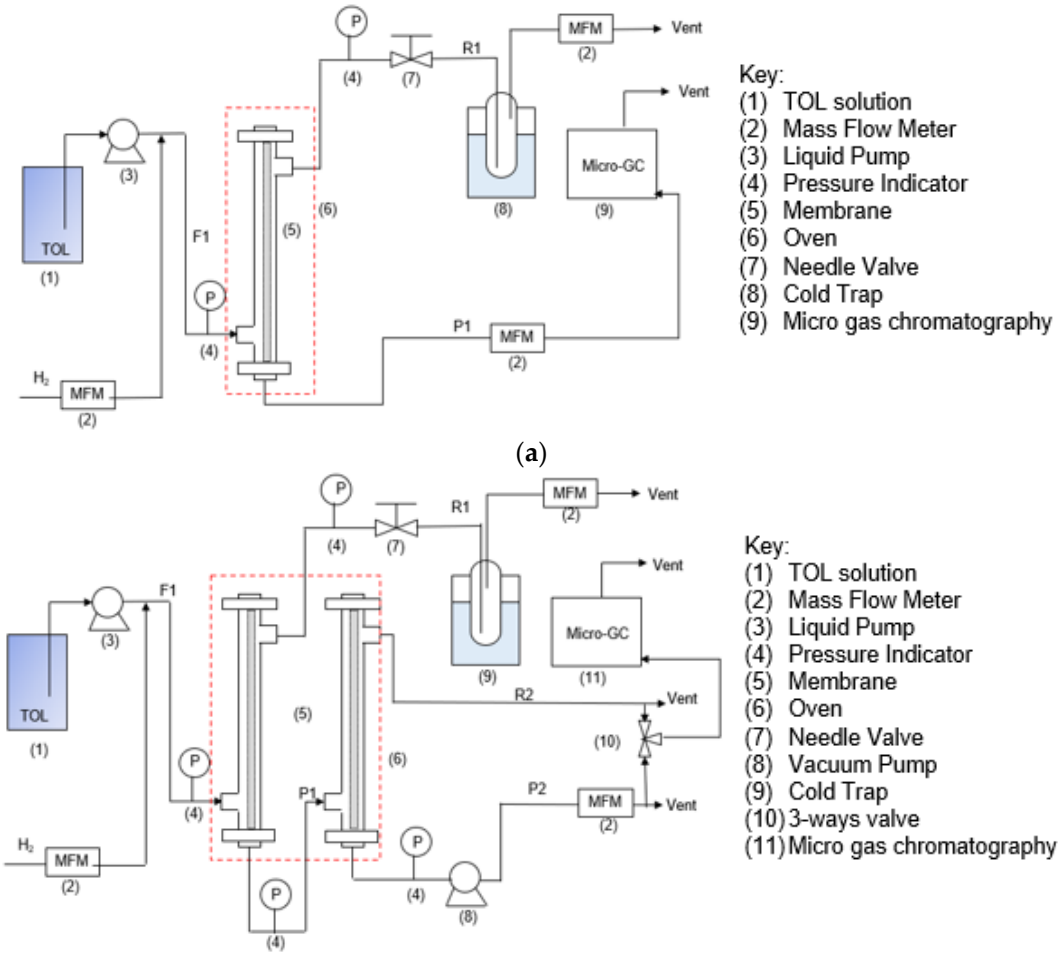


Figure 3. Hydrogen (H_2)/toluene (TOL) separation, (**a**) one-stage and (**b**) two-stage membrane system configurations.

3. Results and Discussion

3.1. Single-Gas Permeation (SGP) and Pore Size Evaluation

To investigate the permeation effectiveness of the in-house BTESE membranes with other inorganic membranes, the SGP was evaluated using He, H_2, N_2, CH_6, CH_4, CF_4, and SF_6 at a permeation temperature of 200 °C. Si-CHA and Si-STT zeolite membranes [31] evaluated at 300 °C and dimethoxydiphenylsilane (DMDPS)-derived CVD silica membranes [32] evaluated at 200 °C were included, as shown in Figure 4. These two membranes

were included in the H_2/TOL separation study; the authors used an almost similar feed mixture gas (TOL/H_2 = 2/98 mol%) to our present study (TOL/H_2 = 3/97 mol%). This condition corresponds to the gas-phase composition after TOL removal by condensation following the methylcyclohexane dehydrogenation process.

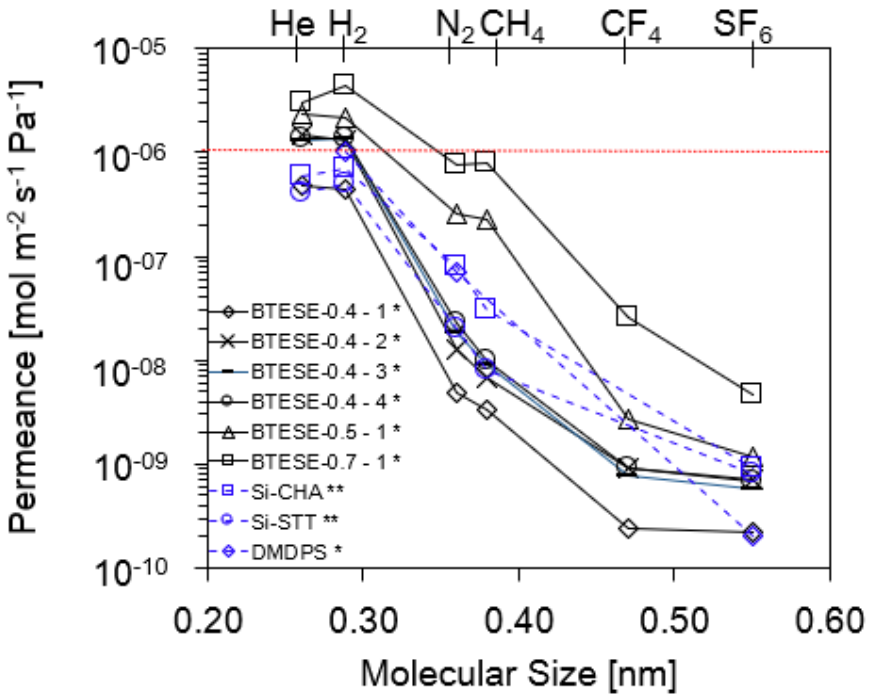


Figure 4. Single gas permeance vs. molecular size (* gas permeation evaluated at 200 °C; ** gas permeation evaluated at 300 °C).

Interestingly, despite variations in pore diameters, all of the in-house BTESE membranes showed a H_2 permeance of more than 10^{-6} mol m^{-2} s^{-1} Pa^{-1}, as shown in Figure 4. The BTESE-0.4-1 membrane showed a H_2 permeance which was lower than other BTESE-0.4 membranes (below 10^{-6} mol m^{-2} s^{-1} Pa^{-1}) and is comparable to that of the Si-CHA [31], Si-STT [31], and DMDPS [32] membranes. However, the permeances of other gases such as N_2, CH_4, CF_4, and SF_6 were higher for both Si-CHA and Si-STT membranes than the BTESE-0.4 type of membrane, demonstrating that both zeolites have a loose pore network compared to BTESE-0.4 membranes. In terms of the DMDPS membrane, it is hard to predict the pore size of this membrane as only a limited number of gases (H_2, N_2, and SF_6) were tested on this membrane, which showed higher N_2 permeance but similar SF_6 permeance to the BTESE-0.4-1 membrane.

Figure 5 demonstrates the permeance ratios of H_2/N_2 and H_2/SF_6 as a function of H_2 permeance. Generally, the performance follows a trade-off relationship for each system (H_2 vs. SF_6 and H_2 vs. N_2). All BTESE membranes have a moderate H_2/N_2 permeance ratio of approximately 5 to 110 but a high and wide range of H_2/SF_6 selectivity around 970–2400. The results indicate that when the pore size of the BTESE membranes drops, the gas permeance ratio increases and H_2 permeance decreases. These results are based on the gas permeation properties and are obtained using the normalized Knudsen-based permeance (NKP) method, which will be discussed later.

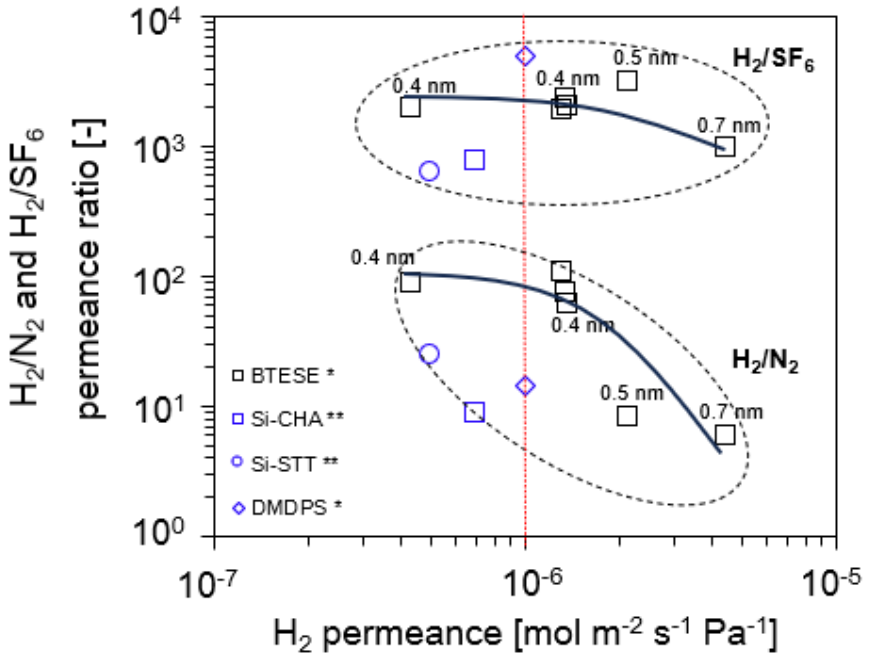


Figure 5. Permeance ratio of H_2/N_2 and H_2/SF_6 vs. H_2 permeance (* gas permeation evaluated at 200 °C; ** gas permeation evaluated at 300 °C).

In the case of the Si-CHA [31] and Si-STT [31] membranes, the H_2/N_2 permeance ratio is 9 and 25, and the H_2/SF_6 permeance ratio, on the other hand, is 778 and 625, respectively. Both gas permeance ratios for the Si-CHA and Si-STT membranes are moderate compared to those of the BTESE-0.4 membrane group. This observation supports our previous statement that Si-CHA and Si-STT membranes had a loose pore network compared to the BTESE membrane group. In comparison to the BTESE membranes itself, a H_2/N_2 permeance ratio ~ 61 to 106 indicates that the BTESE-0.4 membrane group exhibits a smaller pore size compared to the H_2/N_2 permeance ratio < 10 (BTESE-0.5 and BTESE-0.7 membrane groups). The lower H_2/N_2 permeance ratio is attributed to the looser structure of the BTESE membrane (BTESE-0.5-1 and BTESE-0.7-1). Large-pore membranes (BTESE-0.5-1 and BTESE-0.7-1) also exhibit high H_2 permeance due to the low permeation resistance through the membrane. Detailed information on these gas separation properties is summarized in Table 2.

Table 2. Summary of gas permeance, gas permeance ratio, and pore sizes of the BTESE and other inorganic membranes.

Membrane Numbers	H_2 Permeance [10^{-6} mol m^{-2} s^{-1} Pa^{-1}]	Permeance Ratio		NKP [nm]
		H_2/N_2	H_2/SF_6	
BTESE-0.4-1 *	0.43	89	1991	~0.46
BTESE-0.4-2 *	1.33	106	1908	~0.46
BTESE-0.4-3 *	1.36	73	2321	~0.47
BTESE-0.4-4 *	1.38	61	2051	~0.47
BTESE-0.5-1 *	2.15	8	1846	~0.54
BTESE-0.7-1 *	4.45	6	972	~0.73
Si-CHA [31] **	0.70	9	778	~0.55
Si-STT [31] **	0.50	25	625	~0.53
DMDPS [32] *	1.00	14	5000	N/A

* Gas permeation evaluated at 200 °C; ** gas permeation evaluated at 300 °C.

Figure 6a–c illustrate how the NKP approach [33] was used to precisely assess each membrane's pore size. The modified gas translation (GT) model, which was developed by Xiao and Wei [34] and Shelekhin et al. [35] for the purpose of determining membrane pore

sizes of less than 1 nm, is the foundation of this NKP technique. A more detailed explanation of this model can be found elsewhere [33]. NKP is the ratio of the *i*-th component's permeance to the permeance predicted by the Knudsen diffusion mechanism using He, the smallest molecule. The normalized Knudsen-based permeance expression can be produced as follows.

$$NKP = \frac{P_i}{P_{He}} \frac{\sqrt{M_i}}{\sqrt{M_{He}}} = \frac{\left(d_p - d_{k,\,i}\right)^3}{\left(d_p - d_{k,He}\right)^3} exp\left(-\frac{E_{p,\,i} - E_{p,He}}{RT}\right) \quad (8)$$

where d_p is the average pore size of the membrane and $d_{k,\,i}$ is the molecular size of the *i*-th component. The symbols $E_{p,i}$, $E_{p,He}$, R, and T stand for the activation energy of the *i*-th component, He, the gas constant, and the temperature, respectively. To facilitate the evaluation of microporous membrane pore sizes, the current study assumed a small variation in the activation energy of permeation. This led to the following expression for NKP (Equation (9)).

$$NKP = \frac{\left(d_p - d_{k,\,i}\right)^3}{\left(d_p - d_{k,He}\right)^3} \quad (9)$$

Figure 6 shows the NKP plot at 200 °C where the surface flow is negligible. This result confirms that BTESE-0.4 membranes had a smaller pore size distribution.

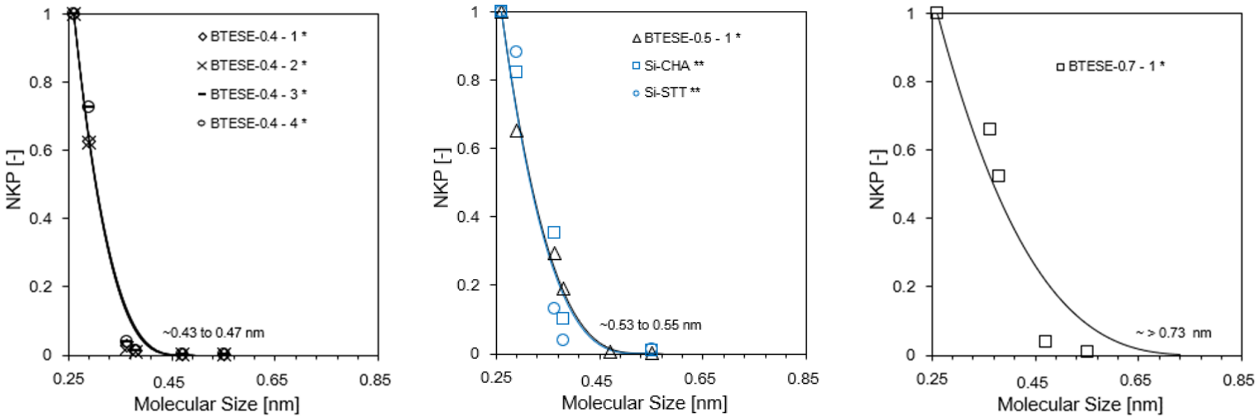


Figure 6. (**a**–**c**) The pore size estimation via the NKP method as a function of the molecular size of permeating gases (symbols and curves indicate the experimental data and the theoretical curves for d_p ~0.7, 0.5 and 0.4 nm, respectively). * Gas permeation in this work was evaluated at 200 °C; ** gas permeation in [31] was evaluated at 300 °C.

3.2. Hydrogen (H_2)/Toluene (TOL) Binary Separation in a One-Stage Membrane Configuration System

The separation performance via a one-stage membrane configuration system is shown in Figure 7a–d. For the 6 h H_2/TOL separation test, the BTESE-0.4-2 membrane, whose pores are around 0.4 nm in size, is shown as a typical example in the figure. The experiment was initiated with single H_2, followed by binary separation (H_2/TOL), and then single H_2. Compared to the initial single H_2 gas permeance, the H2 permeance in the mixed H_2/TOL appears to be slightly lower. However, during the almost 6 h H_2/TOL separation test, the H_2 permeance showed stable values > 10^{-6} mol m^{-2} s^{-1} Pa^{-1}, with low TOL permeance < 10^{-8} mol m^{-2} s^{-1} Pa^{-1}. After the mixed-gas test, H_2 permeance recovered to the same level as the initial H_2 single-gas permeance, as shown in Figure 7a. This finding suggests that TOL molecules did not block the membrane pore network or adsorb on its surface. Figure 7b, c shows the permeate H_2 purity and TOL concentration, which correspond to 99.9 mol% and 900 ppm, respectively. Figure 7d exhibits that the H_2 recovery in the permeate stream was around 0.5, while the TOL recovery in the retentate stream was 0.9. This study revealed that with only one-stage membranes, the H_2 purity in the permeate

stream can be achieved at approximately ~99 mol% for all BTESE membranes, similarly to other inorganic membranes [31,32,34].

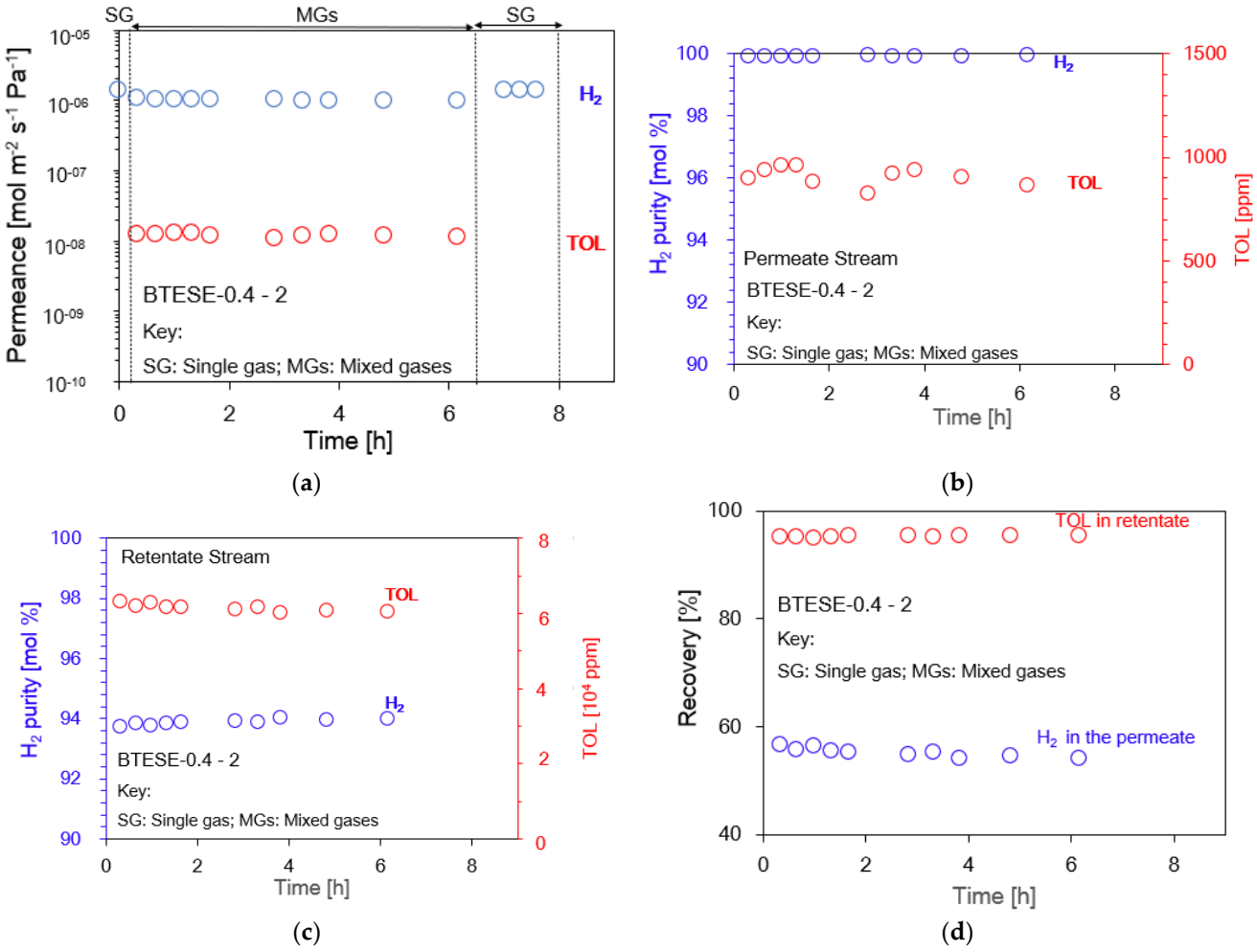


Figure 7. H_2/TOL separation test for one-stage membrane system configuration, (**a**) H_2 and TOL permeance; (**b**) H_2 purity [mol %] and TOL concentration [ppm] in the permeate stream; (**c**) H_2 purity [mol %] and TOL concentration [ppm] in the retentate stream; and (**d**) H_2 recovery in permeate and TOL recovery in retentate stream.

The H_2/TOL and TOL/H_2 permeance ratios versus H_2 permeance of BTESE and other inorganic membranes using a one-stage membrane system are shown in Figure 8. In terms of H_2 permeance and the H_2/TOL permeance ratio, our BTESE membranes continue to be regarded as high-performance membranes based on their performance in comparisons with other membrane materials [31,32,36,37]. The ionic liquid membrane [37] is a TOL-permeable membrane as it exhibits a high TOL/H_2 permeance ratio. However, TOL-permeable membranes are not appropriate for the purification of H_2.

Figure 9 shows the H_2/TOL permeance ratio plotted against the permeance ratios of H_2/N_2 and H_2/SF_6 in order to examine any possible correlation. Both the mixed H_2/TOL and single H_2/N_2 and H_2/SF_6 permeance ratios were measured at 200 °C. The molecular sizes of hydrogen (H_2), nitrogen (N_2), sulfur hexafluoride (SF6), and toluene (TOL) are reportedly 0.29, 0.36, 0.55, and 0.58 nm [14], respectively. Therefore, we assumed it was reasonable to use SF_6 gas as a predictor for TOL permeance. The permeance ratio can be considered a measurement of the pore size distribution of the BTESE membrane; that is, the higher the permeance ratios, the smaller the pore sizes. As can be seen in Figure 9a,b, with an increase in the permeance ratio of H_2/N_2 and H_2/SF_6, the permeance ratio of

H_2/TOL also increased. The membranes with small pore sizes (0.4 nm) are plotted at the top right of both figures, as these membranes possessed high separation performance, and the membranes with the membranes with larger pore sizes are plotted at the bottom left of the figures due to their low permeance ratio.

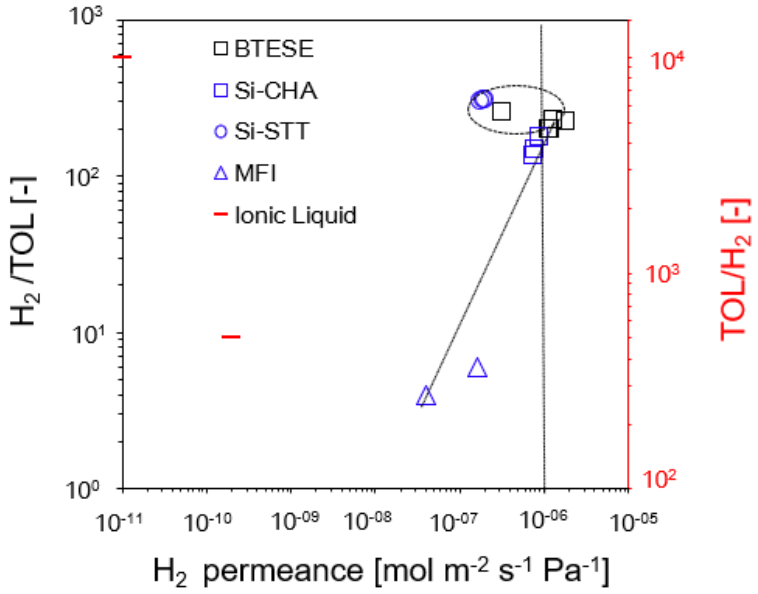
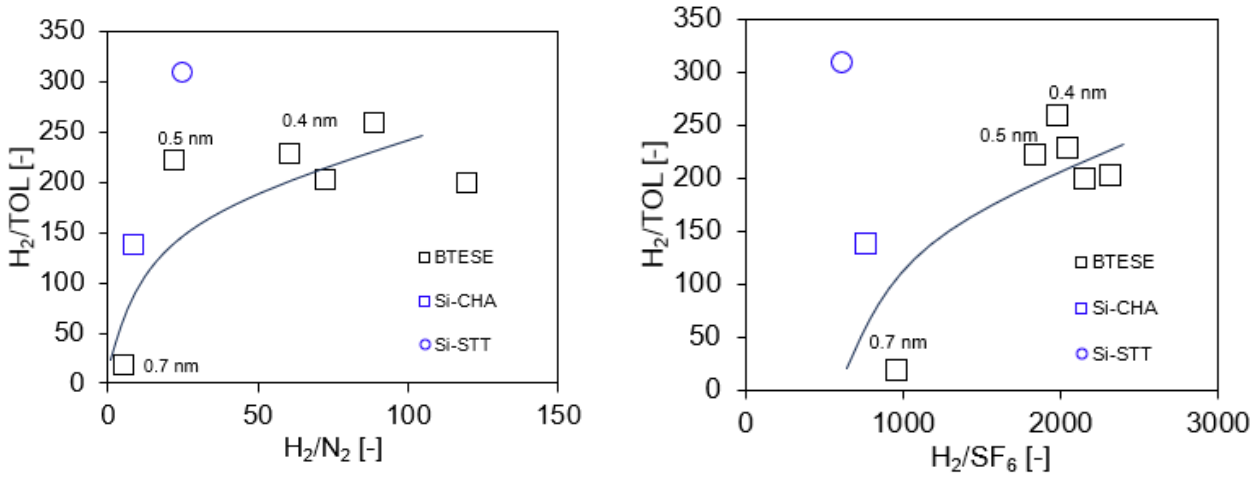


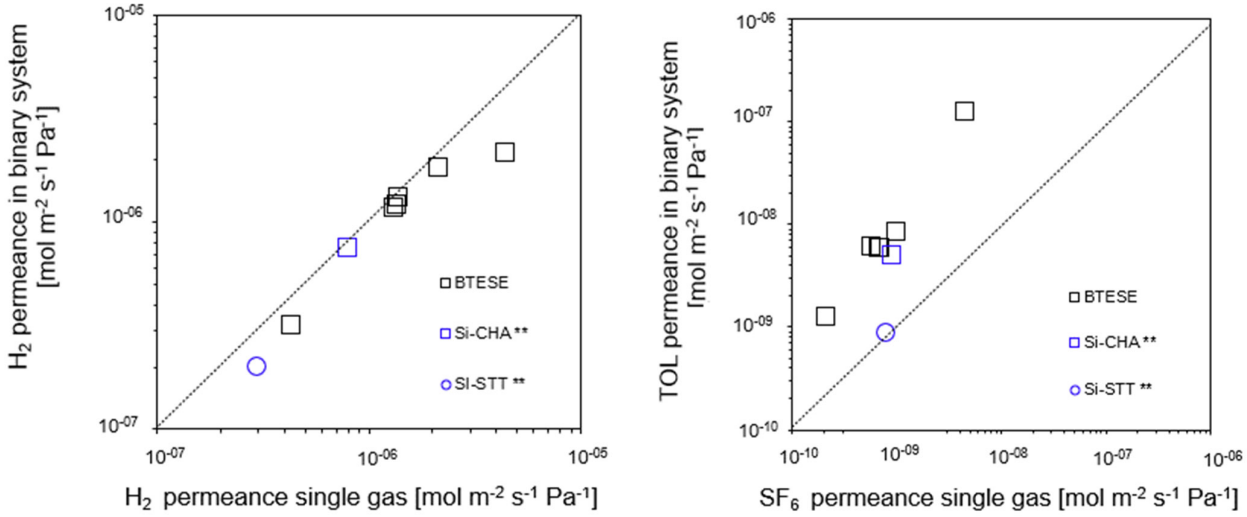
Figure 8. H_2/TOL and TOL/H_2 permeance ratios versus H_2 permeance of BTESE and other inorganic membranes using a one-stage membrane system.



(**a**) (**b**)

Figure 9. Permeance ratio of the mixed H_2/TOL versus single-gas H_2/N_2 (**a**) and permeance ratio of the mixed H_2/TOL versus single-gas H_2/SF_6 (**b**).

Remarkably, Figure 10a shows that the H_2 mixed-gas permeance was slightly lower than the H_2 single-gas permeance for all BTESE membranes as well as Si-CHA and Si-STT zeolites membranes. This is possibly due to the fact the fact that some TOL molecules in the mixed-gas system may have absorbed on the membrane surface as well as blocked the pores of the membranes for H_2 permeation.



(**a**) (**b**)

Figure 10. (**a**) H_2 permeance in binary (H_2/TOL) and single system and (**b**) TOL permeance versus SF_6 permeance (* gas permeation evaluated at 200 °C; ** gas permeation evaluated at 150 °C).

However, upon analyzing the TOL and SF_6 gas permeances, as shown in Figure 10b, we discovered that the TOL permeance was higher than the SF_6 permeance for all BTESE and Si-CHA membranes. Only the Si-STT membrane shows almost the same permeance as TOL and SF_6 gas. Toluene (TOL) and sulfur hexafluoride (SF_6) reportedly have molecular sizes of 0.55 and 0.58 nm, respectively. However, it is possible that TOL's molecular size was smaller than SF_6's. This outcome is consistent with the findings of Niimi et al. [14]. Li et al. [38] reported that the order of permeances was not always correlated with the kinetic diameter. H_2O and NH_3 are claimed to have kinetic diameters between 0.26 and 0.265 nm, which is less than the H2 size of 0.289 nm. At high temperatures (400–500 °C), however, amorphous SiO_2 membranes have consistently demonstrated a higher permeance for H_2 than for either NH_3 or H_2O [38]. The sizes of molecules can be ascertained using a variety of techniques, such as collision diameter and kinetic diameter. According to the findings by Li et al. [38], the appropriate molecular sizes for NH_3 and H_2O were found to be 0.326 nm and 0.2995 nm, respectively. An additional possibility is the impact of penetrating molecular structures and membrane pores. Since TOL is most likely more planar than spherical, it may have been preferred for penetration through the slit-like pores or pinholes that may be present in our BTESE-derived membranes. This might be one reason why our BTESE membranes exhibited a greater permeance for TOL in comparison to SF_6, whose structure is more spherical.

In order to examine the effect of temperature on the BTESE membrane, the BTESE-0.5-1 membrane was tested at different temperatures ranging from 100 to 200 °C, as shown in Figure 10. The feed pressure (P_f) was set at 300 kPaA, and the feed concentrations of H_2 and TOL were set at 97 mol% and 3 mol%, respectively. Figure 11 illustrates the temperature dependencies of the single H_2, mixed-gas H_2, and TOL permeance (bottom figure) and the permeance ratio of H_2/TOL (top figure), respectively. In spite of the gas state (pure or mixed gas), H_2 permeance increased as temperature increased, which indicates an activated diffusion tendency [14], whereas TOL permeance decreased as temperature increased in such a manner as to indicate surface diffusion. This result is in line with the finding by Niimi et al. [14] that the effect of TOL adsorption on H_2 permeation was small at high temperatures. Therefore, it can be concluded that a high-temperature operation is preferable to achieve a high H_2 permeance and a high H_2/TOL permeance ratio.

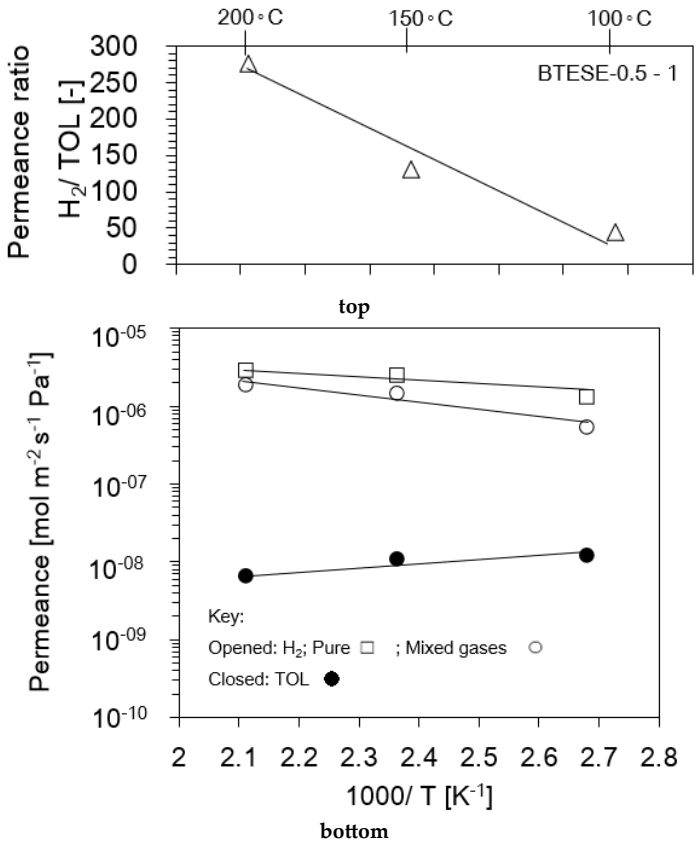


Figure 11. The H_2 and TOL permeance dependence on temperature (**bottom**) and H_2/TOL permeance ratio (**top**).

As for the comparison with other membranes, our organosilica BTESE membranes showed high H_2 permeance compared to the other zeolite membranes [31,32,36]. Most of our BTESE membranes exhibit promising H_2 permeance over 1×10^{-6} mol m^{-2} s^{-1} Pa^{-1} after 60 min of the H_2/TOL separation test, with the exception of the BTESE-0.4-1 membrane, which has the smallest pore network. BTESE-0.5-1 membrane with a pore size around 0.5 nm exhibits a remarkable performance of H_2 recovery > 80% and H_2 purity > 99.9% in the permeate stream. Si-STT membranes showed slightly high H_2/TOL compared to the BTESE membranes, which was attributed to the adsorption capability of the Si-STT membranes. Reportedly, Si-STT allows toluene to adsorb without preventing H_2 from passing through its two-dimensional pore systems, which have seven- and nine-membered ring windows (0.24×0.35 and 0.37×0.53 nm^2, respectively) [31,37,39–41].

Seshimo et al. [32] reported that using a feed mixture of H_2/TOL (98/2 mol%) at an operating temperature of 200 °C, their dimethoxydiphenylsilane (DMDPS)-derived silica membrane achieved stable purification of hydrogen higher than 99.99% purity and TOL concentrations of 70 ppm in the permeate stream. However, the H_2 permeance for this membrane was below 1×10^{-6} mol m^{-2} s^{-1} Pa^{-1}. We also compared our BTESE membrane H_2/TOL performance with a supported ionic liquid membrane (SILM) and ionic liquid organosilica (ILOS) membranes. These two membranes are reported to have a high TOL/H_2 separation factor of over 1000–17,000 [37]; however, the H_2/TOL separation factor is below 1 for these both membranes, and the H_2 permeance ranges from 1×10^{-10} to 1×10^{-11} mol m^{-2} s^{-1} Pa^{-1} at operating conditions of feed pressure (P_f: 220 kPaA) and an operating temperature of 70 °C, which seems useful to concentrate TOL but unsuitable to purify H_2. The detailed information on these H_2/TOL separation test properties is shown in Table 3.

Table 3. H_2/TOL separation test performance of BTESE and other inorganic membranes via one-stage membrane process.

Membrane Code	Pressure [kPaA]		Temperature [°C]	H_2/TOL Concentration Feed mol [%]	Permeate Stream						Retentate Stream		Refs
					Permeance [10^{-6} mol m^{-2} s^{-1} Pa^{-1}]		H_2/TOL [-]	H_2 Purity [mol %]	H_2 Recovery [%]	TOL Concentration [ppm]	TOL Recovery [%]	TOL Concentration [ppm]	
	Feed	Permeate			H_2	TOL							
BTESE-0.4-1	200	101.3	200	97/3	0.32	0.00123	258	99.972	8.8	280	98.2	32,668	[This work]
BTESE-0.4-2	200	101.3	200	97/3	1.16	0.00586	198	99.957	30.2	428	98.5	41,730	[This work]
BTESE-0.4-2	300	111.0	200	97/3	0.96	0.01104	87	99.914	53.9	859	95.3	60,149	[This work]
BTESE-0.4-3	200	101.3	200	97/3	1.21	0.00602	200	99.958	34.1	418	95.9	43,977	[This work]
BTESE-0.4-4	200	101.3	200	97/3	1.31	0.00579	227	99.963	38.7	375	100.1	46,972	[This work]
BTESE-0.5-1	200	101.3	200	97/3	1.83	0.00830	221	99.956	50.2	441	96.1	56,490	[This work]
BTESE-0.5-1	300	101.3	200	97/3	1.73	0.00681	253	99.944	81.5	557	88.0	127,303	[This work]
BTESE-0.7-1	200	101.3	200	97/3	2.15	0.12300	17	99.456	60.0	5441	92.0	62,293	[This work]
Si-CHA	300	101.3	90	98/2	0.88	0.00500	176	99.989	N/A	N/A	N/A	N/A	[31]
Si-CHA	300	101.3	120	98/2	0.77	0.00520	148	99.987	N/A	N/A	N/A	N/A	[31]
Si-CHA	300	101.3	150	98/2	0.75	0.00550	136	99.984	N/A	N/A	N/A	N/A	[31]
Si-STT	300	101.3	90	98/2	0.18	0.00060	300	99.992	N/A	N/A	N/A	N/A	[31]
Si-STT	300	101.3	120	98/2	0.19	0.00062	306	99.992	N/A	N/A	N/A	N/A	[31]
Si-STT	300	101.3	150	98/2	0.20	0.00065	308	99.991	N/A	N/A	N/A	N/A	[31]
DMDPS	N/A	N/A	200	98/2	0.90	N/A	N/A	99.996					[32]
MFI	300	101.3	120	98/2	0.04	0.00940	4	N/A	N/A	N/A	N/A	N/A	[36]
MFI	300	101.3	200	98/2	0.16	0.02500	6	N/A	N/A	N/A	N/A	N/A	[36]
SILM	220	200	70	N/A	0.0002	0.10	0.0020	N/A	N/A	N/A	N/A	N/A	[37]
ILOS	220	200	70	N/A	0.00001	0.10	0.0001	N/A	N/A	N/A	N/A	N/A	[37]

3.3. Hydrogen (H_2)/Toluene (TOL) Binary Separation in a Two-Stage Membrane Configuration System

Due to the overall performance of our BTESE membrane in terms of TOL concentration in the permeate stream, it still falls short of our desired level, which is less than 200 ppm. In order to reach the intended goal, the two membranes were placed in a cascade (Figure 3b). The BTESE-0.5-1 membrane was chosen as the first membrane, while the BTESE-0.4-2 membrane was chosen as the second membrane for the two-stage membrane configuration system.

Figure 12 reveals the time course of separation performance of the two-stage membrane configuration system consisting of the BTESE-0.5-1 and BTESE-0.4-2 membranes for an almost 6 h H_2/TOL separation test. After the 6 h H_2/TOL separation test, the single H_2 permeance can still recover to the same value as the initial value of the H_2 single gas permeance for one- and two-stage membranes, as shown in Figure 12a1,a2. In addition, our target was that the H_2 permeance should be more than 1×10^{-6} mol m^{-2} s^{-1} Pa^{-1}. As can be seen after 6 h, the H_2 permeance for both membranes is still above 1×10^{-6} mol m^{-2} s^{-1} Pa^{-1}. It can be observed that the H_2 purity, TOL concentration, and H_2 and TOL recovery in permeate and retentate for both one- and two-stage membranes were stable for the 6 h H_2/TOL separation test, as shown in Figure 12b1,b2. The BTESE-0.5-1 membrane enabled H_2 purity > 99.9 mol% in the permeate (P1) stream; nevertheless, the TOL concentration remained higher than 200 ppm. Due to this reason, we purified the P1 stream with another membrane to reduce the TOL concentration to 200 ppm. By applying the two-stage membrane system, the TOL concentration was reduced to be below 200 ppm, and at the same time, the H_2 purity was still >99.9 mol% (Figure 12b2). Figure 12c1,c2 show H_2 recovery in permeate and TOL recovery in retentate in the first and second membranes. More than 80% recovery of H_2 and TOL was achieved in the first membrane. Approximately 40% H_2 recovery with a purity of >99.99% was achieved via two-stage configurations.

Meanwhile, Figure 13 shows the time course of the performance of the two-stage membrane configuration system at three different temperatures (100, 150, and 200 °C) for a 7 h H_2/TOL separation test. It can be seen that at 150 and 200 °C, the H_2 permeance for both membranes exceeds 1×10^{-6} mol m^{-2} s^{-1} Pa^{-1}. At temperatures of 150 and 200 °C, the H_2 purity in the P2 stream is over 99.99 mol%, while the TOL concentration is around 50 ppm. In addition to this, it can be observed that the final product for the H_2 purity and TOL concentration in the P2 stream as a function of time at temperatures between 150 and 200 °C seems to reach a steady state, probably 2 h after supplying the H_2/TOL gas mixtures. However, at 100 °C, H_2 purity and TOL concentration in the P2 stream are not up to the same performance values as at 150 and 200 °C. This is due to the low permeance of H_2 gas via the one- and two-stage membrane modules, which resulted in a low permeance ratio of H_2/TOL ~below 50 and 20 (Figure 13a), respectively. Hence, the H_2/TOL separation test took a longer time to reach its steady state, probably because some TOL molecules gradually blocked the pore network of the membranes; hence, a longer time is required for H_2 gas to pass through. In addition, there is no additional pressure applied to the two-stage membrane; hence, it can be considered another possible reason for this observation. Based on the final result, 150 and 200 °C are the recommended temperatures for H_2/TOL separation via the BTESE membrane. Detailed operating data of the two-stage membrane configurations at 200 °C using the BTESE-0.5-1 and BTESE-0.4-2 membrane configuration systems are shown in Figure 14.

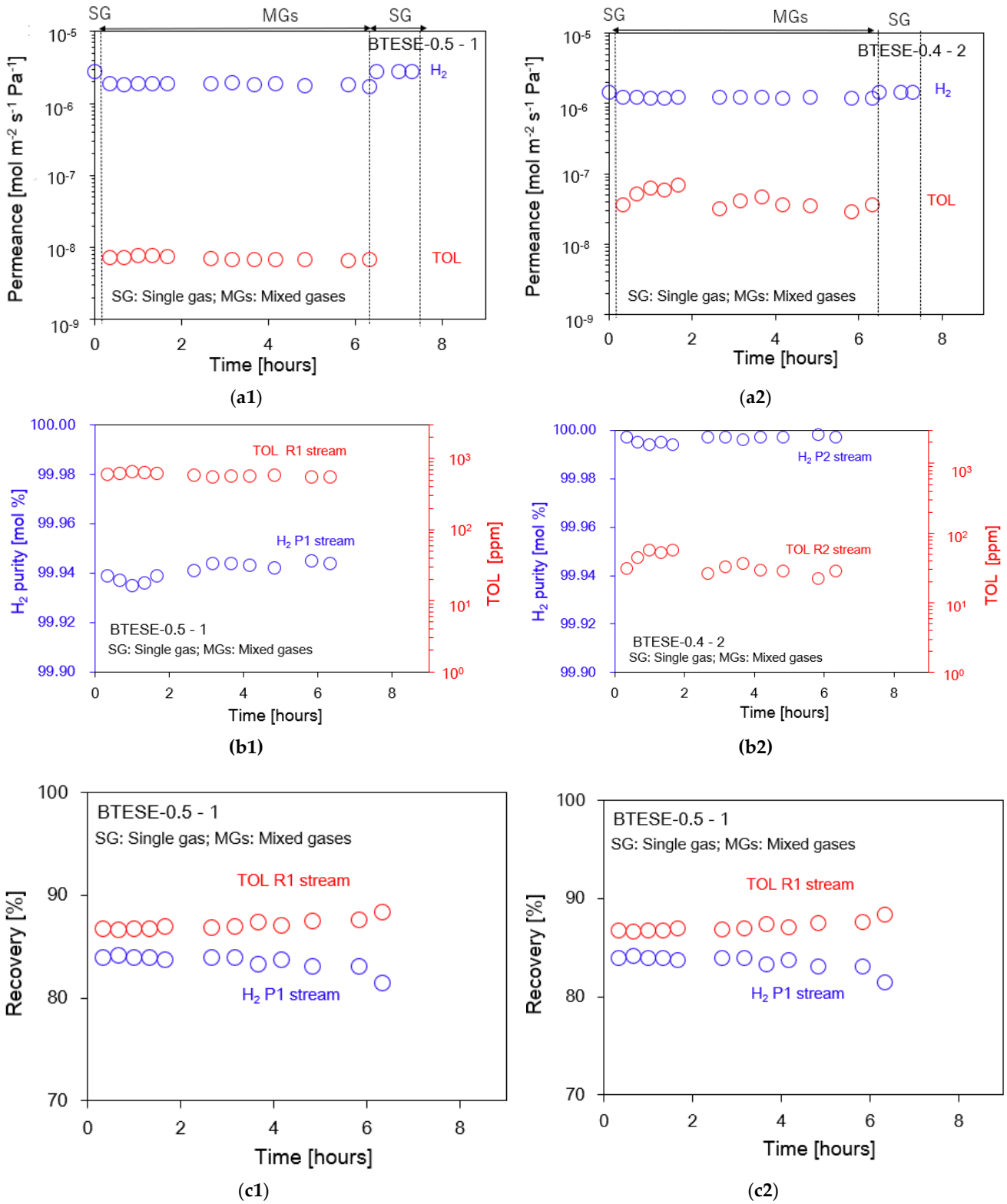


Figure 12. H_2/TOL separation test for two-stage membrane system configuration. (**a**) H_2 and TOL permeance in the permeate P1 streams (**a1**) and permeate P2 streams (**a2**); (**b**) H_2 purity [mol %] and TOL concentration [ppm] in the permeate (P1 and R1) stream (**b1**) and the permeate (P2 and R2) stream (**b2**); (**c**) H_2 recovery in permeate (P1) and TOL recovery (R1) in retentate streams (**c1**) and permeate (P2) and TOL recovery (R2) in retentate streams (**c2**).

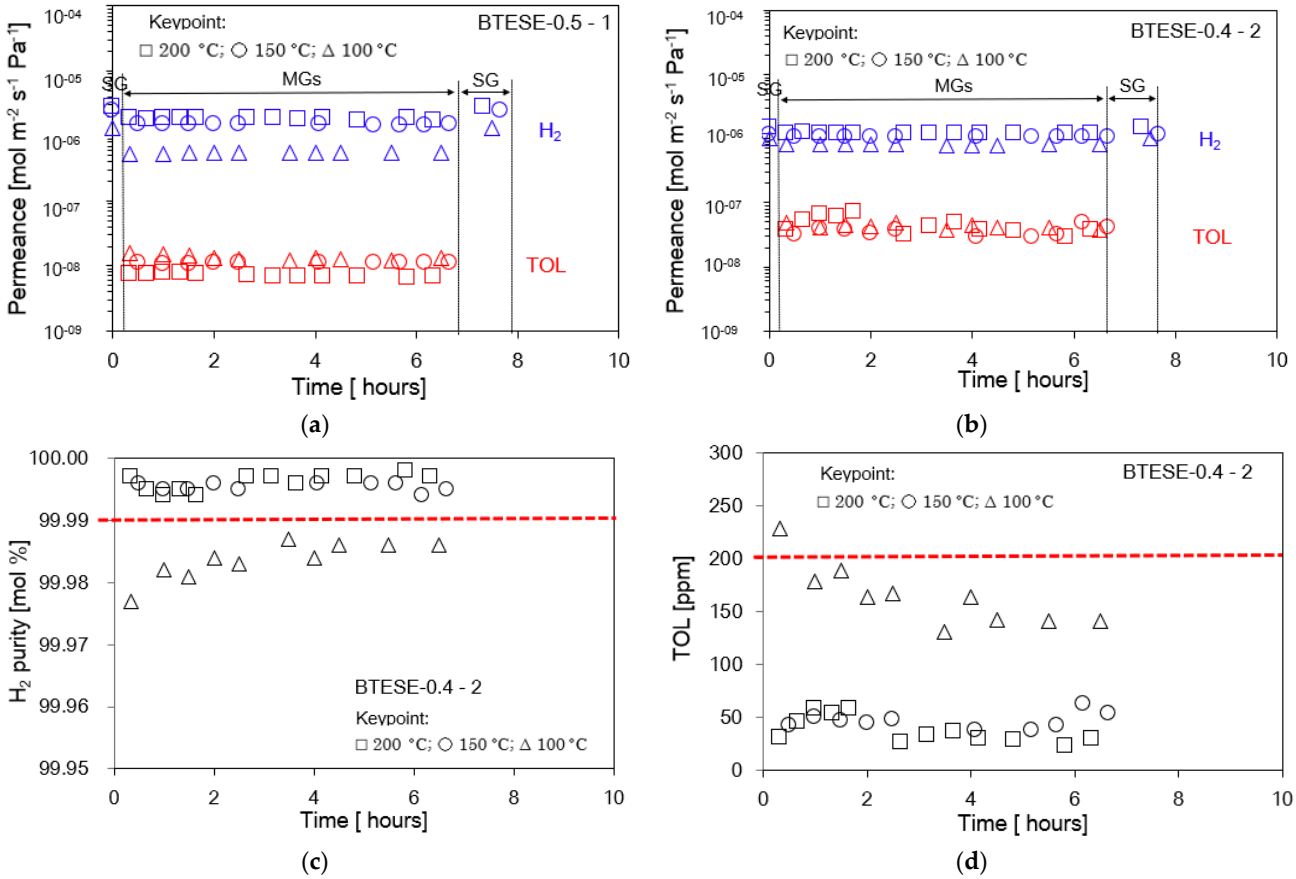


Figure 13. H_2/TOL separation test at different temperatures (100, 150, 200 °C) for different membrane configurations: (**a**) H_2 and TOL permeance in the first-stage membrane; (**b**) H_2 and TOL permeance in the second-stage membrane; (**c**) H_2 purity [mol %] in the second-stage membrane; and (**d**) TOL concentration in permeate stream in the second-stage membrane.

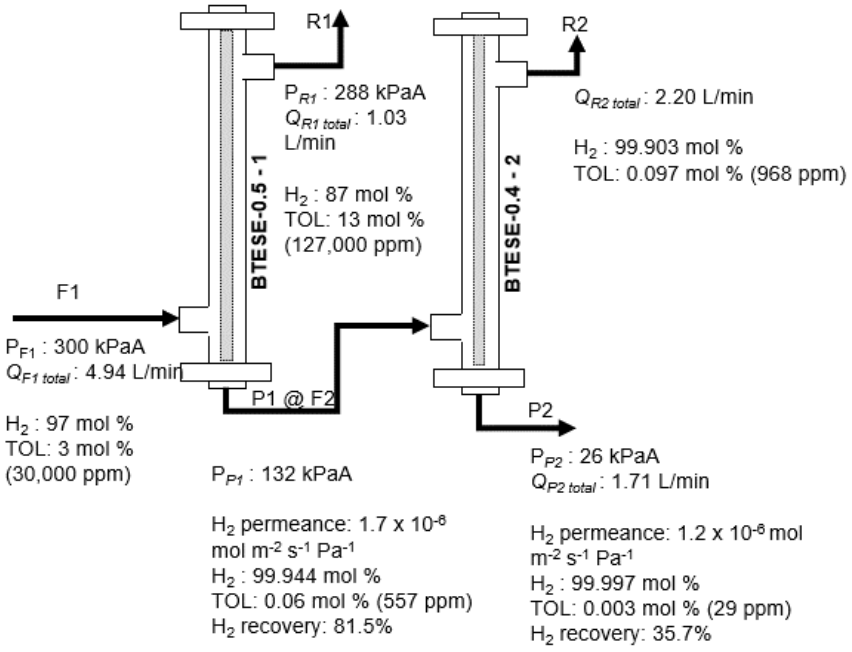


Figure 14. Schematic diagram of the H_2/TOL separation test for the BTESE-0.5-1 and BTESE-0.4-2 membrane configuration systems at 200 °C.

4. Conclusions

The present study has effectively demonstrated that we can adjust the pore size distribution of our BTESE membranes by changing the number of coating layers. Despite variations in pore diameters, all of the in-house BTESE membranes showed a H_2 permeance greater than 10^{-6} mol m^{-2} s^{-1} Pa^{-1}, with $H_2/SF_6 > 1000$. Additionally, the present study also marks the successful preparation of 40 cm long BTESE membranes for H_2/TOL separation. The BTESE membranes showed a reasonable correlation for H_2/TOL against H_2/N_2 and H_2/SF_6. By applying the two-stage BTESE membrane system configuration, it has been shown that the TOL concentration in the permeate stream can be lowered below 200 ppm while the H_2 purity is >99.999 mol% and stable for 6 h of operation.

Author Contributions: S.M.I.: methodology, formal analysis, investigation—experimental, writing—original draft preparation, writing—review and editing; X.Y.: formal analysis—H_2/TOL system/micro GC equipment setting and setup; S.M.: formal analysis—membrane preparation; K.M.: formal analysis—BTESE solution preparation; F.S.: formal analysis—micro GC equipment setting and setup; S.O.L.: formal analysis—membrane characterization; T.T.: supervision, conceptualization, writing—review and editing; K.-i.S.: supervision, conceptualization, funding acquisition. All authors have read and agreed to the published version of the manuscript.

Funding: This research was funded by the METI Monozukuri R&D Support Grant Program for SMEs Grant Number JPJ005698.

Institutional Review Board Statement: Not applicable.

Data Availability Statement: The raw data supporting the conclusions of this article will be made available by the authors on request.

Acknowledgments: This article is based on results obtained from a project, JPJ005698, subsidized by the Ministry of Economy, Trade and Industry (METI).

Conflicts of Interest: Authors S.M.I., X.Y., K.M., S.M., F.S., S.O.L., T.T. and K.-i.S. were employed by the company eSep Inc. The remaining authors declare that the research was conducted in the absence of any commercial or financial relationships that could be construed as a potential conflict of interest.

References

1. EU. Hydrogen and Fuel Cells—A Vision of Our Future. High Level Group Draft Report v4.8. Publications Office. 2003. Available online: https://inis.iaea.org/search/search.aspx?orig_q=RN:37121708 (accessed on 22 July 2024).
2. Levin, D.B.; Chahine, R. Challenges for renewable hydrogen production from biomass. *Int. J. Hydrogen Energy* **2010**, *35*, 4962–4969. [CrossRef]
3. Rambhujun, N.; Salman, M.S.; Wang, T.; Pratthana, C.; Sapkota, P.; Costalin, M.; Lai, Q.; Aguey-Zinsou, K.F. Renewable hydrogen for the chemical industry. *MRS Energy Sustain.* **2020**, *7*, E33. [CrossRef] [PubMed]
4. IEA. The Future of Hydrogen. 2019. Available online: https://www.iea.org/reports/the-future-of-hydrogen (accessed on 22 July 2024).
5. Giuli, M. Geopolitics of the Energy Transition. In *Handbook of Energy Transitions*; CRC Press: Boca Raton, FL, USA, 2022; pp. 41–59.
6. Liu, C.; Zhang, X.; Zhai, J.; Li, X.; Guo, X.; He, G. Research progress and prospects on hydrogen separation membranes. *Clean Energy* **2023**, *7*, 217–241. [CrossRef]
7. Bernado, G.; Arau'jo, T.; da Silva Lopes, T.; Sousa, J.; Mendes, A. Recent advances in membrane technologies for hydrogen purification. *Int. J. Hydrogen Energy* **2020**, *45*, 7313–7338. [CrossRef]
8. Adhikari, S.; Fernando, S. Hydrogen Membrane Separation Techniques. *Ind. Eng. Chem. Res.* **2006**, *45*, 875–881. [CrossRef]
9. Freeman, B.D.; Pinnau, I. Gas and liquid separations using membranes: An overview. In *Advanced Materials for Membrane Separations*; Pinnau, I., Freeman, B.D., Eds.; ACS Symposium Series; ACS: Washington, DC, USA, 2004; Volume 876, pp. 1–21.
10. Kayı, H.; Kaya, P.; Kurt, T.; Mirza, E.S.; Topuz, B. Ti-substituted organosilica membranes for H_2 sieving: Sol-gel and DFT insights. *Int. J. Hydrogen Energy* **2024**, *65*, 496–504. [CrossRef]
11. Moriyama, N.; Nagasawa, H.; Kanezashi, M.; Tsuru, T. Improved performance of organosilica membranes for steam recovery at moderate-to-high temperatures via the use of a hydrothermally stable intermediate layer. *J. Membr. Sci.* **2021**, *620*, 118895. [CrossRef]
12. Sawamura, K.; Okamoto, S.; Todokoro, Y. Development of Mass Production Technology of Highly Permeable Nano-Porous 534 Supports for Silica-Based Separation Membranes. *Membranes* **2019**, *9*, 103. [CrossRef]
13. Ibrahim, S.M.; Sawamura, K.; Mishina, K.; Yu, X.; Salak, F.; Miyata, S.; Moriyama, N.; Nagasawa, H.; Kanezashi, M.; Tsuru, T. Bis(triethoxysilyl)ethane (BTESE)–Organosilica Membranes for H_2O/DMF Separation in Reverse Osmosis (RO): Evaluation and

Correlation of Subnanopores via Nanopermporometry (NPP), Modified Gas Translation (mGT) and RO Performance. *Membranes* **2024**, *14*, 8. [CrossRef]
14. Niimi, T.; Nagasawa, H.; Kanezashi, M.; Yoshioka, T.; Ito, K.; Tsuru, T. Preparation of BTESE-derived organosilica membranes for catalytic membrane reactors of methylcyclohexane dehydrogenation. *J. Membr. Sci.* **2014**, *455*, 375–383. [CrossRef]
15. Raza, W.; Yang, J.; Wang, J.; Saulat, H.; He, G.; Lu, J.; Zhang, Y. HCl modification and pervaporation performance of BTESE membrane for the dehydration of acetic acid/water mixture. *Sep. Purif. Technol.* **2020**, *235*, 116102. [CrossRef]
16. Ibrahim, S.M.; Nagasawa, H.; Kanezashi, M.; Tsuru, T. Organosilica bis(triethoxysilyl)ethane (BTESE) membranes for gas permeation (GS) and reverse osmosis (RO): The effect of preparation conditions on structure, and the correlation between gas and liquid permeation properties. *J. Membr. Sci.* **2017**, *526*, 242–251. [CrossRef]
17. Xu, R.; Liu, Q.; Ren, X.; Lin, P.; Zhong, J. Tuning the Pore Structures of Organosilica Membranes for Enhanced Desalination Performance via the Control of Calcination Temperatures. *Membranes* **2020**, *10*, 392. [CrossRef] [PubMed]
18. Song, H.; Wei, Y.; Qi, H. Tailoring pore structures to improve the permselectivity of organosilica membranes by tuning calcination parameters. *J. Mater. Chem. A* **2017**, *5*, 24657–24666. [CrossRef]
19. Ren, Y.; He, D.; Wang, T.; Qi, H. Effect of ZIF-7 doping content on H_2/CO_2 separation performance of 1,2-bis(triethoxysilyl)ethane-derived organosilica membranes. *Sep. Purif. Technol.* **2023**, *311*, 123347. [CrossRef]
20. Zhang, H.; He, D.; Niu, S.; Qi, H. Tuning the microstructure of organosilica membranes with improved gas permselectivity via the co-polymerization of 1,2-bis(triethoxysilyl) ethane and 1,2-bis(triethoxysilyl)methane. *Int. J. Hydrogen Energy* **2021**, *46*, 17221–17230. [CrossRef]
21. Osman, A.I.; Mehta, N.; Elgarahy, A.M.; Hefny, M.; Al-Hinai, A.; Al-Muhtaseb, A.H.; Rooney, D.W. Hydrogen production, storage, utilisation and environmental impacts: A review. *Environ. Chem. Lett.* **2022**, *20*, 153–188. [CrossRef]
22. Massarweh, O.; Al-Khuzaei, M.; Al-Shafi, M.; Bicer, Y.; Abushaikha, A.S. Blue hydrogen production from natural gas reservoirs: A review of application and feasibility. *J. CO_2 Util.* **2023**, *70*, 102438. [CrossRef]
23. Noussan, M.; Raimondi, P.P.; Scita, R.; Hafner, M. The role of green and blue hydrogen in the energy transition—A technological and geopolitical perspective. *Sustainability* **2021**, *13*, 298. [CrossRef]
24. Alhumaidan, F.; Cresswell, D.; Garforth, A. Hydrogen Storage in Liquid Organic Hydride: Producing Hydrogen Catalytically from Methylcyclohexane. *Energy Fuels* **2011**, *25*, 4217–4234. [CrossRef]
25. Seshimo, M.; Urai, H.; Sasa, K.; Nishino, H.; Yamaguchi, Y.; Nishida, R.; Nakao, S. Bench-Scale Membrane Reactor for Methylcyclohexane Dehydrogenation using Silica Membrane Module. *Membranes* **2021**, *11*, 326. [CrossRef] [PubMed]
26. Ali, J.K.; Baiker, A. Dehydrogenation of methylcyclohexane to toluene in a pilot-scale membrane reactor. *Appl. Catal. A-Gen.* **1997**, *155*, 41–57. [CrossRef]
27. Kreuder, H.; Boeltken, T.; Cholewa, M.; Meier, J.; Pfeifer, P.; Dittmeyer, R. Heat storage by the dehydrogenation of methylcyclohexane—Experimental studies for the design of a microstructured membrane reactor. *Int. J. Hydrogen Energy* **2016**, *41*, 12082–12092. [CrossRef]
28. Li, G.; Niimi, T.; Kanezashi, M.; Yoshioka, T.; Tsuru, T. Equilibrium shift of methylcyclohexane dehydrogenation in a thermally stable organosilica membrane reactor for high-purity hydrogen production. *Int. J. Hydrogen Energy* **2013**, *38*, 15302–15306. [CrossRef]
29. Acharya, D.; Ng, D.; Xie, Z. Recent Advances in Catalysts and Membranes for MCH Dehydrogenation: A Mini Review. *Membranes* **2021**, *11*, 955. [CrossRef] [PubMed]
30. Zhang, X.L.; Akamatsu, K.; Nakao, S. Hyrogen Separation in Hydrogen-Methylcylohexane-Toluene Gaseous Mixtures through Triphenylmethoxysilane-derived Silica Membranes Prepared by Chemical Vapor Deposition. *Ind. Eng. Chem. Res.* **2016**, *55*, 5395–5402. [CrossRef]
31. Kida, K.; Maeta, Y.; Kuno, T.; Yogo, K. Hydrogen Purification from Chemical Hydride Using Pure Silica Zeolite Membranes. *Chem. Lett.* **2017**, *46*, 1724–1727. [CrossRef]
32. Seshimo, M.; Saito, T.; Akamatsu, K.; Segawa, A.; Nakao, S. Influence of toluene vapor on the H_2-selective performance of dimethoxydiphenylsilane-derived silica membranes prepared by the chemical vapor deposition method. *J. Membr. Sci.* **2012**, *415–416*, 51–56. [CrossRef]
33. Lee, H.L.; Kanezashi, M.; Shimomura, Y.; Yoshioka, T.; Tsuru, T. Evaluation and fabrication of pore size tune silica membranes with tetraethoxydimetyl disiloxane for gas separation. *AIChE J.* **2011**, *57*, 2755–2765. [CrossRef]
34. Xiao, J.; Wei, J. Diffusion mechanism of hydrocarbons in zeolites-I. Theory. *Chem. Eng. Sci.* **1992**, *47*, 1123–1142. [CrossRef]
35. Shelekhin, A.B.; Dixon, A.G.; Ma, Y.H. Theory of gas diffusion and permeation in inorganic molecular-sieve membranes. *AIChE J.* **1995**, *41*, 58–67. [CrossRef]
36. Kumakiri, I.; Qiu, L.; Liu, N.; Tanaka, K.; Kita, H.; Sato, T.; Nishida, R. Application of MFI Zeolite Membrane Prepared with Fluoride Ions to Hydrogen/Toluene. *Sep. J. Chem. Eng. Jpn.* **2016**, *49*, 753–755. [CrossRef]
37. Hirota, Y.; Maeda, Y.; Yamamoto, Y.; Miyamoto, M.; Nishiyama, N. Organosilica membrane with ionic liquid properties for separation of toluene/H_2 mixture. *Materials* **2017**, *10*, 901. [CrossRef] [PubMed]
38. Li, G.; Kanezashi, M.; Yoshioka, T.; Tsuru, T. Ammonia decomposition in catalystic membrane reactors: Simulation and experimental studies. *AIChE J.* **2013**, *59*, 168–179. [CrossRef]
39. Imasaka, S.; Nakai, A.; Araki, S.; Yamamoto, H. Syntesis and Gas Permeation Properties of STT-type Zeolite Membranes. *J. Jpn. Pet. Inst.* **2018**, *61*, 263–271. [CrossRef]

40. Camblor, M.A.; Diaz-Cabanas, M.J.; Perez-Pariente, J.; Teat, S.J.; Clegg, W.; Shannon, J.; Lightfoot, P.; Wright, P.A.; Morris, R.E. SSZ-23: An Odd Zeolite with Pore Openings of Seven and Nine Tetrahedral Atoms. *Angew. Chem. Int. Ed.* **1998**, *37*, 2122–2126. [CrossRef]
41. Funke, H.H.; Argo, A.M.; Falconer, J.L.; Noble, R.D. Separations of Cyclic, Branched and Linear Hydrocarbon Mixtures through Silicate Membranes. *Ind. Eng. Chem. Res.* **1997**, *36*, 137–143. [CrossRef]

Disclaimer/Publisher's Note: The statements, opinions and data contained in all publications are solely those of the individual author(s) and contributor(s) and not of MDPI and/or the editor(s). MDPI and/or the editor(s) disclaim responsibility for any injury to people or property resulting from any ideas, methods, instructions or products referred to in the content.